On the consistency of the SPH gradient with a Boundary Integral Method for solid wall modelling

V. Degand [a, *], J. Michel [a], D. Le Touzé [a], G. Oger [a]
[a] Nantes Université, École Centrale Nantes, CNRS, LHEEA, UMR 6598, F-44000 Nantes, France
[*] valentin.degand@ec-nantes.fr

The consistency of the SPH gradient with a Boundary Integral Method (BIM) for solid wall modelling is studied numerically. In particular, the discretization error due to both quadratures with fluid particles and solid wall faces are quantified with respect to their respective characteristic length Δx and Δl. The influence of particles disorder is also investigated.

I. Introduction

The Smoothed Particle Hydrodynamics (SPH) method was introduced in 1977 for problems of astronomical interest, set in an unbounded spatial domain. Since then, the SPH method proved to be also advantageous for the simulation of hydraulics problems. However, in these applications, the fluid domain is often bounded by solid walls. Thus, the question of solid wall Boundary Conditions (BCs) enforcement became a grand challenge for the SPH community [1].

The various existing methods for solid wall modelling in SPH can be classified into three main categories: repulsive forces, fictitious particles and Boundary Integral Methods (BIMs). This last category refers to methods in which a boundary integral term over the wall surface is derived and discretized. Various BIMs have been derived in the past 20 years (see *e.g.* [2]–[8]) with the goal of modelling solid wall boundaries of complex geometry.

If the conservation properties of the SPH method with BIMs is often discussed [2], [6], [9], its consistency is less addressed in the literature. The recent work [10] on the consistency of SPH with a BIM compares different correction factors. In the latter work, the characteristic length of a face Δl was taken as ten times finer than the characteristic length of a particle Δx to avoid any quadrature error on the boundary integral term.

However, using such a fine discretization for the boundary integral quadrature could lead to added computational costs for no significant accuracy gain. The goal of the present work is thus to study the consistency of the SPH gradient with a BIM and to see how both parameters Δl and Δx influence the discretization error in order to find an optimal relation between them. Firstly, errors for the SPH gradient with a BIM are formalized showing the dependency on both Δl and Δx. Then, numerical analyses are performed on a simple setup in order to study the convergence of the errors with respect to both parameters Δl and Δx.

II. Errors for the SPH gradient with a BIM

A. Smoothing error

Let $\Omega \subset \mathbb{R}^n$ be a fluid domain of dimension $n \in \mathbb{N}^*$ assumed to be only bounded by a solid wall $\partial\Omega$. Let ϕ be a scalar field defined on Ω. Using the BIM formalism, the smoothed gradient of ϕ is defined as the sum of an integral over the fluid domain and an integral over the solid wall boundary:

$$\langle \boldsymbol{\nabla}\phi \rangle = \langle \boldsymbol{\nabla}\phi \rangle^{\Omega} + \langle \boldsymbol{\nabla}\phi \rangle^{\partial\Omega} \tag{1}$$

with for each location $\boldsymbol{x} \in \Omega$:

$$\langle \boldsymbol{\nabla}\phi \rangle^{\Omega}(\boldsymbol{x}) = \frac{1}{\gamma(\boldsymbol{x})} \left(\int_{\Omega} \phi(\boldsymbol{x}') \boldsymbol{\nabla} W(\boldsymbol{x} - \boldsymbol{x}') d^n \boldsymbol{x}' \right) \tag{2}$$

$$\langle \boldsymbol{\nabla}\phi \rangle^{\partial\Omega}(\boldsymbol{x}) = \frac{1}{\gamma(\boldsymbol{x})} \left(\int_{\partial\Omega} \phi(\boldsymbol{x}') W(\boldsymbol{x} - \boldsymbol{x}') \boldsymbol{n}_{\boldsymbol{x}'} d^{n-1} \boldsymbol{x}' \right) \tag{3}$$

where the smoothing kernel $W : \mathbb{R}^d \longrightarrow \mathbb{R}^+$ is a radially symmetric function with compact support of radius R, $\boldsymbol{n}$ is the unit normal pointing outward Ω, and γ is the wall normalization factor as defined in [2].

The error field related to this smoothing approximation is:

$$\boldsymbol{\varepsilon}_{smooth} = \boldsymbol{\nabla}\phi - \langle \boldsymbol{\nabla}\phi \rangle \tag{4}$$

B. Discretization error

The solid wall $\partial\Omega$ is assumed piecewise planar so there is no ambiguity nor error associated to the definition of its geometry. The fluid domain Ω is discretized as a set of particles $j \in \mathcal{P}$ with characteristic length Δx, whereas the solid wall boundary $\partial\Omega$ is discretized as a set of faces $s \in \mathcal{S}$ with characteristic length Δl. The discrete smoothed gradient is then defined as:

$$\langle \boldsymbol{\nabla}\phi \rangle^{\Delta x, \Delta l} = \langle \boldsymbol{\nabla}\phi \rangle^{\Omega, \Delta x} + \langle \boldsymbol{\nabla}\phi \rangle^{\partial\Omega, \Delta l} \tag{5}$$

with for each location $\boldsymbol{x}_i \in \Omega$:

$$\langle \boldsymbol{\nabla}\phi \rangle_i^{\Omega, \Delta x} = \frac{1}{\gamma_i} \sum_{j \in \mathcal{P}} \phi_j \boldsymbol{\nabla} W_{ij} \omega_j \tag{6}$$

$$\langle \boldsymbol{\nabla}\phi \rangle_i^{\partial\Omega, \Delta l} = \frac{1}{\gamma_i} \sum_{s \in \mathcal{S}} \phi_s W_{is} \boldsymbol{n}_s \omega_s \tag{7}$$

where $\omega_j \sim \Delta x^n$ and $\omega_s \sim \Delta l^{n-1}$ are the quadrature weights.

The error field related to this discretization is:

$$\varepsilon_{discr} = \langle \nabla\phi \rangle - \langle \nabla\phi \rangle^{\Delta x, \Delta l} \tag{8}$$

$$= \underbrace{\langle \nabla\phi \rangle^{\Omega} - \langle \nabla\phi \rangle^{\Omega, \Delta x}}_{\varepsilon_{\Delta x}} + \underbrace{\langle \nabla\phi \rangle^{\partial\Omega} - \langle \nabla\phi \rangle^{\partial\Omega, \Delta l}}_{\varepsilon_{\Delta l}} \tag{9}$$

where $\varepsilon_{\Delta x}$ is the error field related to the quadrature of the integral over the fluid domain and $\varepsilon_{\Delta l}$ to the quadrature of the boundary integral.

III. Numerical analysis

A. Numerical setup

The goal of this section is to study the influence of both discretization parameters Δx and Δl on $\varepsilon_{\Delta x}$, $\varepsilon_{\Delta l}$ and ε_{discr}. To this end, a simple geometrical configuration is considered in 2D with the classical orthonormal coordinate system $(O, \boldsymbol{e}_x, \boldsymbol{e}_y)$. A planar wall boundary of normal $\boldsymbol{n} = \boldsymbol{e}_x$ is set along the $(O, \boldsymbol{e}_y)$ axis, and the half-plane $\mathbb{R}^+ \times \mathbb{R}$ is filled with a fluid region. The wall is discretized with equally spaced faces of length Δl whereas the fluid region is discretized with equally spaced particles of surface Δx^2. This Cartesian particles distribution can be perturbed according to a normal law with standard deviation δ in order to investigate the influence of particle disorder.

Also, to evaluate quantities at different distances to the wall $d \in [0, R]$, probes are placed on a segment of length R orthogonal to the wall as shown in Fig. 1.

In the following, all the quantities with a length dimension are non-dimensionalized with respect to R.

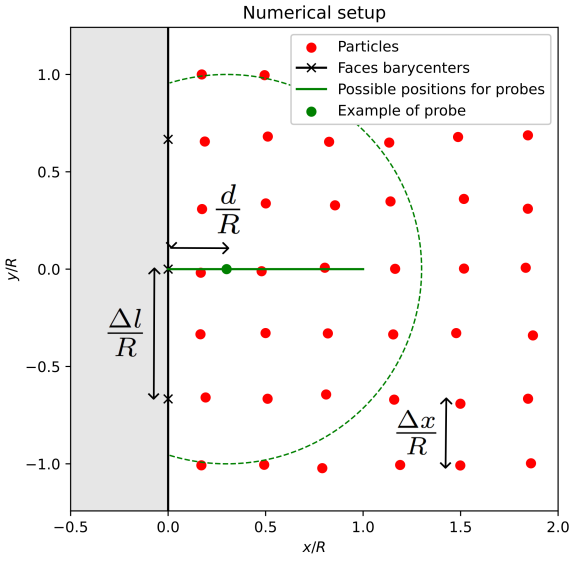

Fig. 1. Domain discretization for $R/\Delta x = 3$, $R/\Delta l = 1.5$, $\delta = 0.05$.

The chosen kernel is the $\mathcal{C}^2$ Wendland kernel, whose wall renormalization factor γ is computed analytically as in [11]. Numerical investigations are performed on a simple affine field ϕ_1 varying only along the normal direction to the wall, which is representative of an hydrostatic pressure field:

$$\forall (x, y) \in \mathbb{R}^+ \times \mathbb{R} : \quad \phi_1(x, y) = x + 1 \tag{10}$$

The terms constituting the SPH gradient of ϕ_1 along $\boldsymbol{n}$ and computed with the discretized domain of Fig. 1 are plotted in Fig. 2 as an illustration.

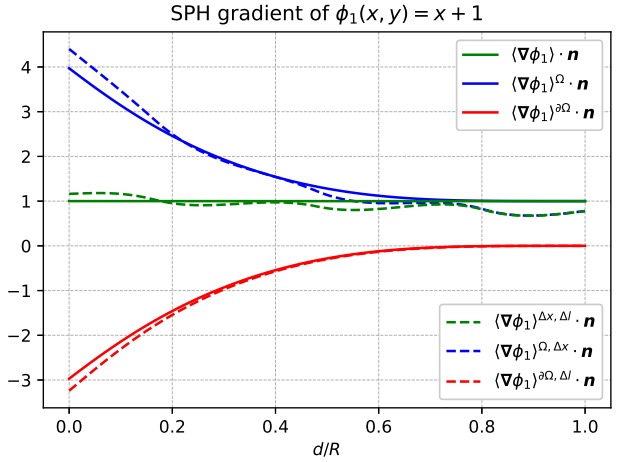

Fig. 2. Smoothed gradient of ϕ_1 (green) with integral term over fluid domain (blue) and boundary integral term (red). Dashed lines are their discretizations.

B. Convergence of $\varepsilon_{\Delta x}$ and $\varepsilon_{\Delta l}$

The convergence of $\varepsilon_{\Delta x}$ and $\varepsilon_{\Delta l}$ are studied at the probe located on the wall ($d/R = 0$). In order to get relative errors at this point, the quantities considered in Fig. 3 are:

$$E_{\Delta x} = \left| \frac{\langle \nabla\phi \rangle^{\Omega} \cdot \boldsymbol{n} - \langle \nabla\phi \rangle^{\Omega, \Delta x} \cdot \boldsymbol{n}}{\langle \nabla\phi \rangle^{\Omega} \cdot \boldsymbol{n}} \right| \tag{11}$$

$$E_{\Delta l} = \left| \frac{\langle \nabla\phi \rangle^{\partial\Omega} \cdot \boldsymbol{n} - \langle \nabla\phi \rangle^{\partial\Omega, \Delta l} \cdot \boldsymbol{n}}{\langle \nabla\phi \rangle^{\partial\Omega} \cdot \boldsymbol{n}} \right| \tag{12}$$

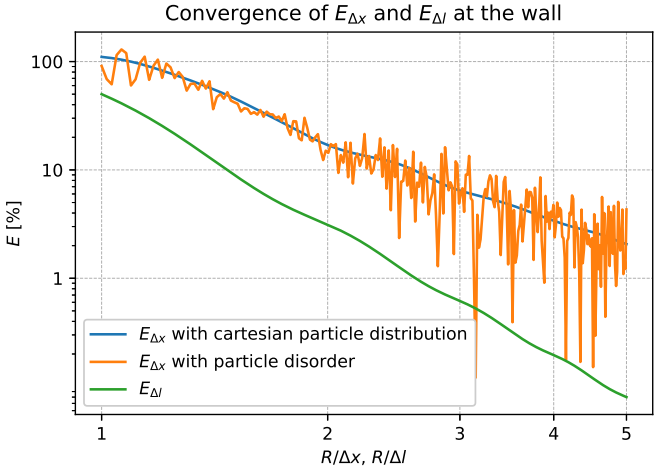

Fig. 3. Convergence of $E_{\Delta x}$ and $E_{\Delta l}$ at the wall.

The main result here is that, at the wall, the rate of convergence of the boundary integral is higher than the rate of convergence of the integral over the fluid domain.

C. Relative influence of $\varepsilon_{\Delta x}$ and $\varepsilon_{\Delta l}$ in ε_{discr}

In the previous section, rates of convergence for both $\varepsilon_{\Delta x}$ and $\varepsilon_{\Delta l}$ have been compared, indicating a faster convergence for the boundary integral quadrature. The question is now how both of these errors terms contribute to ε_{discr} in terms of absolute magnitude. The final goal is to find a good trade-off in the sizes Δx and Δl to make both errors magnitudes comparable, which would be optimal in terms of computational costs (avoiding an over refinement of the solid wall boundary).

To this purpose, ε_{discr} is studied at the probe located on the wall ($d/R = 0$) with the scalar quantity:

$$E_{discr} = \langle \boldsymbol{\nabla} \phi \rangle \cdot \boldsymbol{n} - \langle \boldsymbol{\nabla} \phi \rangle^{\Delta x, \Delta l} \cdot \boldsymbol{n} \tag{13}$$

The evolution of this quantity with respect to both discretization parameters is plotted in Fig. 4.

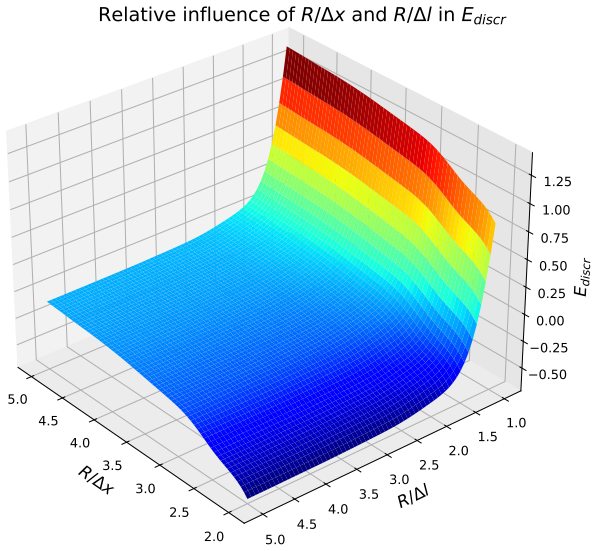

Fig. 4. Convergence of E_{discr} with respect to $R/\Delta x$ and $R/\Delta l$, with no particle disorder ($\delta = 0$).

The first remark here is that the discretization error tends to vanish when the discretization is fine enough for both particles and faces, as theoretically expected. Moreover, a fine discretization of particles together with a coarse discretization of faces makes the discretization error dominated by the boundary integral quadrature error. Conversely, a fine discretization of faces together with a coarse discretization of particles leads to a discretization error dominated by the particles quadrature error. The results were similar in the presence of particles disorder.

Now, in practice, the $R/\Delta x$ ratio is often fixed by practitioners with flow physics considerations and by computational resources limitations. The particles quadrature error being fixed by the choice of this ratio $R/\Delta x$, it is interesting to search for a corresponding $R/\Delta l$ ratio for which the faces quadrature error has the same magnitude. Indeed, any finer discretization in faces would be computationally costly and would result in a negligible accuracy improvement because the discretization error would be dominated by the particles quadrature error. The results linking the ratio $R/\Delta x$ to the corresponding optimal ratio $R/\Delta l$ are given in I.

TABLE I
OPTIMAL LINK BETWEEN $R/\Delta l$ AND $R/\Delta x$ RATIOS TO MAKE PARTICLES QUADRATURE AND FACES QUADRATURE ERRORS OF THE SAME MAGNITUDE.

$R/\Delta x$	2	2.5	3	3.5	4
Corresponding $R/\Delta l$	1.25	1.35	1.51	1.63	1.77
Related $\Delta l/\Delta x$ ratio	1.6	1.85	2	2.14	2.26

IV. Conclusion and Future Work

The consistency of the SPH gradient with a BIM for solid wall modelling has been studied. In particular, the convergence of the boundary integral quadrature has been shown to be faster than the convergence of the particles quadrature. Moreover, it has been shown that for a given $R/\Delta x$ ratio, a corresponding value of $R/\Delta l$ ratio can be found to make both particles and faces quadrature errors of the same magnitude.

Preliminary results in 3D indicate similar error behaviours, and will be extended to other fields, more complex boundary shapes, and to other SPH derivatives (such as the SPH divergence, and the classical symmetric and antisymmetric variants will be performed).

References

[1] Vacondio, R., Altomare, C., De Leffe, M., Hu, X., Le Touzé, D., Lind, S., ..., Souto-Iglesias, A. (2021). Grand challenges for smoothed particle hydrodynamics numerical schemes. Computational Particle Mechanics, 8, 575-588.

[2] Kulasegaram, S., Bonet, J., Lewis, R. W., Profit, M. (2004). A variational formulation based contact algorithm for rigid boundaries in two-dimensional SPH applications. Computational Mechanics, 33, 316-325.

[3] Feldman, J., Bonet, J. (2007). Dynamic refinement and boundary contact forces in SPH with applications in fluid flow problems. International journal for numerical methods in engineering, 72(3), 295-324.

[4] Marongiu, J. C., Leboeuf, F., Caro, J., Parkinson, E. (2010). Free surface flows simulations in Pelton turbines using an hybrid SPH-ALE method. Journal of Hydraulic Research, 48(sup1), 40-49.

[5] De Leffe, M., Le Touzé, D., Alessandrini, B. (2009). Normal flux method at the boundary for SPH. In 4th Int. SPHERIC Workshop (SPHERIC 2009).

[6] Ferrand, M., Laurence, D. R., Rogers, B. D., Violeau, D., Kassiotis, C. (2013). Unified semi-analytical wall boundary conditions for inviscid, laminar or turbulent flows in the meshless SPH method. International Journal for Numerical Methods in Fluids, 71(4), 446-472.

[7] Macia, F., González, L. M., Cercos-Pita, J. L., Souto-Iglesias, A. (2012). A boundary integral SPH formulation: consistency and applications to ISPH and WCSPH. Progress of Theoretical Physics, 128(3), 439-462.

[8] Chiron, L., De Leffe, M., Oger, G., Le Touzé, D. (2019). Fast and accurate SPH modelling of 3D complex wall boundaries in viscous and non viscous flows. Computer Physics Communications, 234, 93-111.

[9] Mayrhofer, A., Rogers, B. D., Violeau, D., Ferrand, M. (2013). Investigation of wall bounded flows using SPH and the unified semi-analytical wall boundary conditions. Computer Physics Communications, 184(11), 2515-2527.

[10] Boregowda, P., Liu, G. R. (2023). On the accuracy of SPH formulations with boundary integral terms. Mathematics and Computers in Simulation, 210, 320-345.

[11] Leroy, A., Violeau, D., Ferrand, M., Kassiotis, C. (2014). Unified semi-analytical wall boundary conditions applied to 2-D incompressible SPH. Journal of Computational Physics, 261, 106-129.